BIOLOGICAL RESEARCH CENTRE
HUNGARIAN ACADEMY OF SCIENCES, SZEGED
INSTITUTE OF BIOPHYSICS

AND

DOCTORAL SCHOOL OF THEORETICAL MEDICINE
UNIVERSITY OF SZEGED

# TARGETING THE BLOOD-BRAIN BARRIER WITH SOLID AND VESICULAR NANOPARTICLES DECORATED WITH LIGANDS OF SOLUTE CARRIERS

Summary of the Ph.D. Thesis

**Mária Mészáros**

Supervisors:

Mária A. Deli, M.D., Ph.D., D.Sc.

Szilvia Veszelka, Ph.D.




SZEGED

2019

## 1. INTRODUCTION

The blood-brain barrier (BBB) is the major obstacle to prevent potential neuropharmaceuticals, especially new biopharmacons, nucleic acids, peptide or protein drugs, to reach their targets in the central nervous system (CNS). Therefore, the pharmaceutical treatment of most CNS disorders, like stroke, brain tumors and neurodegenerative diseases including Alzheimer's and Parkinson's diseases, is difficult. Several clinical trials ended with failure because of the low penetration of biological drugs across the BBB. The rapidly expanding nanotechnology could offer new solutions to solve this problem. Nanoparticles (NPs) are colloidal systems, in the range of 1-1000 nm, which consist of macromolecular components or metals to carry drugs or bioactive materials (Fig. 1).

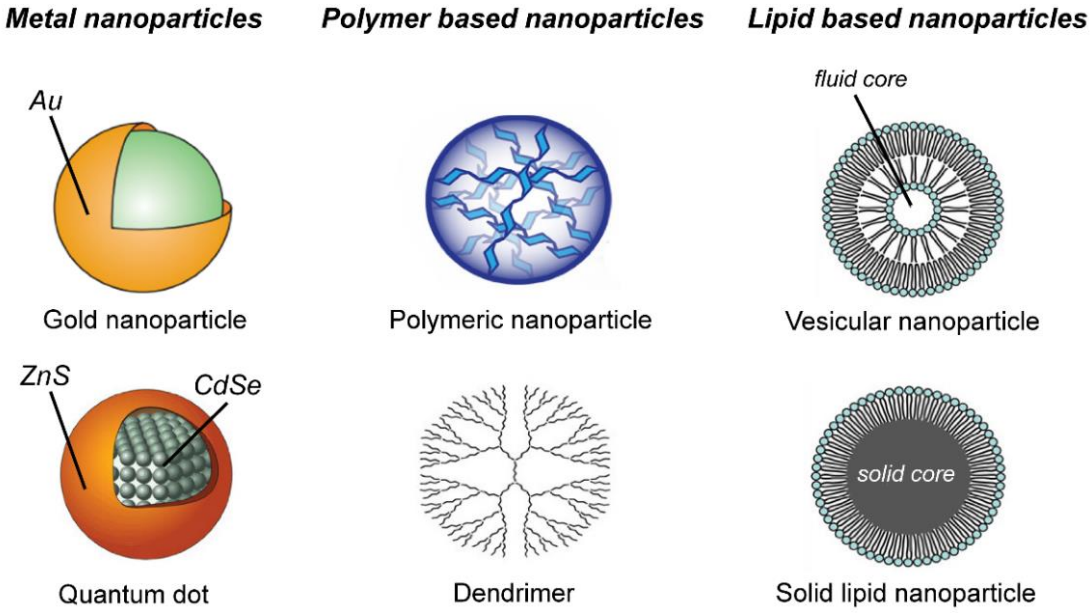


***Figure 1.*** *Major nanoparticle types applied for drug delivery research*

Drug encapsulation in NPs alone is not enough for their successful delivery to the CNS. In order to elevate the permeability of nanocarriers across the BBB specific targeting is needed. Various essential influx transport systems are expressed on the cerebral endothelium playing a physiological role in nutrient delivery. These influx transport systems, especially the solute carriers (SLCs) of the BBB can potentially be exploited to shuttle nanocarriers to the brain.

SLC transporters are actively investigated as drug targets and the number of drug candidates developed for these carriers and reaching clinical trials increases steadily. However, this pathway is not fully utilized for drug delivery and for targeted NPs in particular. Among the SLCs, the expression level of glucose transporter GLUT1 (SLC2A1) is the highest at the

BBB, but other members of the SLC2A family are also present. Glucose analogs have a potential to be efficient and selective targeting ligands for both solid and vesicular nanocarriers to cross the BBB. The number and expression level of SLCs transporting amino acids across the BBB are also high. Neutral amino acids, like alanine, serine and cysteine, are transported by carriers belonging to the sodium-coupled neutral amino acid transporter families (SNAT/SLC38A and ASCT/SLC1A), but alanine, a ligand of these transporters has not been described as a BBB specific targeting ligand of NPs.

SLCs also provide the brain with vitamins. The sodium-dependent multivitamin transporter (SMVT/SLC5A6) is responsible for the transport of biotin (vitamin B7) across the BBB. Biotin has long been used for ligation techniques, imaging and diagnostics based on the strong interaction between biotin and avidin. Biotin-avidin technology has a potential to be applied for targeted drug therapy of tumors. However, biotin has not yet been tested as a potential targeting ligand of NPs to cross brain endothelial cells.

## 2. AIMS

Effective CNS drug targeting with NPs is an unsolved problem. Our main purpose was to design nanocarrier systems for elevating the penetration of cargo molecules across the BBB. Since SLCs are highly and specifically expressed at the BBB, our hypothesis was that NPs with SLC ligands, especially dual ligand combinations will increase the brain endothelial uptake and permeability of the cargo across the BBB. Therefore the major aims of our experiments were:

(I) To verify the gene expression levels of selected SLCs in isolated brain microvessels and *in vitro* BBB models

(II) To test biotin and glutathione as targeting ligands for polystyrene SNPs on a culture BBB model

(III) To prepare and characterize non-ionic surfactant based vesicular NPs loaded with large biomolecule serum albumin as a cargo and targeted with single or dual combination of SLC ligands and glutathione

(IV) To investigate niosomes on cellular viability, uptake and permeability of cargo using a BBB culture model

(V) To reveal the possible mechanisms of the cellular uptake process and the role of the brain endothelial surface charge

(VI) To examine the brain penetration of fluorescent cargo encapsulated in single- and dual SLC ligand-targeted niosomes by optical imaging *in vivo*

## 3. MATERIALS AND METHODS

### 3.1. Animals

Animal studies were performed following the regulations of the 1998. XXVIII. Hungarian law and the EU Directive 2010/63/EU (permit numbers: XVI./03835/001/2006, XVI./834/2012). For the *in vivo* experiments ten week old male CD1-Foxn1nu nude mice (Charles River Laboratories, Wilmington, MA, USA) were used. For the microvessel and primary cell isolations brain tissues were obtained from 3-month-old (microvessels), 3-week-old (brain endothelial cells and pericytes) or newborn (glial cells) outbred Wistar rats (Harlan Laboratories, United Kingdom) of both sexes.

### 3.2. Cell cultures

The following cell cultures were used for our *in vitro* experiments: human cerebral microvascular endothelial cell line (hCMEC/D3), primary rat brain endothelial cells (RBECs) in monoculture and in triple co-culture BBB model with pericytes and astrocytes (Fig. 2).

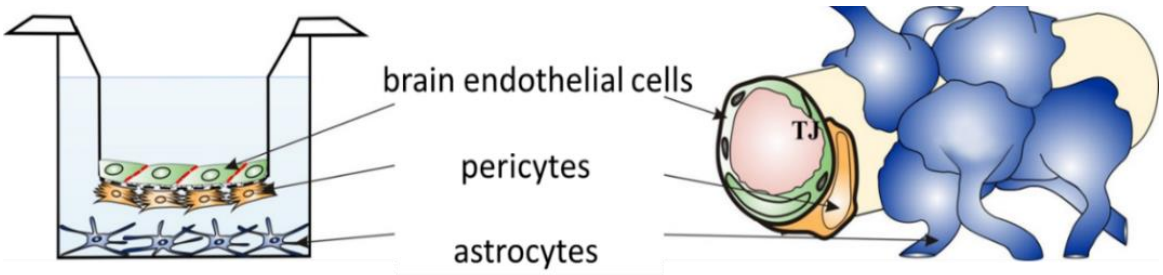


***Figure 2****. Schematic drawing of the BBB triple co-culture model and the structure of a brain capillary. TJ: tight junction.*

### 3.3. Gene expression study of solute carriers

RNA was isolated from rat brain microvessels, hCMEC/D3 cells and RBECs from a triple co-culture and cDNA was synthetized. The expression of the genes of transporters for glucose (*GLUT1/SLC2A1*, *GLUT3/SLC2A3*, *GLUT5/SLC2A5*), for alanine (sodium-coupled neutral amino acid transporters *SNAT1/SLC38A1*, *SNAT2/SLC38A2*, *SNAT3/SLC38A3*, *SNAT5/SLC38A5*, *ASCT1/SLC1A4*, *ASCT2/SLC1A5*) and for biotin (sodium-dependent multivitamin transporter *SMVT/SLC5A6*) were analyzed by quantitative PCR.

### 3.4. Experiments with targeted solid nanoparticles

#### 3.4.1. Functionalization and characterization of solid nanoparticles

Red fluorescent solid nanoparticles (SNPs) made from polystyrene and labeled with neutravidin were used for the study. The SNPs were functionalized with biotin (SNP-B) or biotinylated-glutathione (SNP-B-GSH) and characterized for particle size and zeta potential using dynamic light scattering. The morphology of nanoparticles was visualized by scanning electron microscopy.

#### 3.4.2. Viability measurements and cellular uptake of solid nanoparticles

The viability and metabolic activity of hCMEC/D3 after treatment with SNPs was verified with MTT-test. To measure the cellular uptake of SNPs hCMEC/D3 cells were seeded to 24-well plates. The confluent monolayers were incubated with SNP, SNP-B and SNP-B-GSH at 150 μg/mL concentration for 4 or 8 h at 37 ºC. After incubation the cells were washed with ice cold phosphate buffer (PBS) and lysed in Triton X-100 detergent. The fluorescence intensity of cell lysates was measured with a spectrofluorometer at 488 nm excitation and 605 nm emission wavelengths. The cellular uptake of the fluorescent SNPs was visualized with a confocal laser scanning microscope.

#### 3.4.3. Permeability measurement of solid nanoparticles

For permeability studies the hCMEC/D3 cells were seeded onto collagen coated 12-well tissue culture inserts and cultured for 5 days. The integrity of the monolayers was checked by Evans blue-labeled bovine serum albumin (EBA, 67 kDa; 0.167 mg/mL EB, 10 mg/mL BSA) permeability marker molecule. The cells were treated with SNP, SNP-B or SNP-B-GSH diluted in culture medium at 150 μg/mL concentration in the upper, donor compartments (0.5 mL) for 8 h. After incubation samples were collected from the lower or acceptor compartments (1.5 mL) and measured with a spectrofluorometer at 488 nm excitation and 605 nm emission wavelengths for the SNPs and at 584 nm excitation and 680 nm emission wavelengths for EBA to calculate the apparent permeability coefficients ($P_{app}$, cm/s).

### 3.5. Experiments with targeted vesicular nanoparticles

#### 3.5.1. Functionalization and characterization of niosomes

Niosomes, the vesicular NPs used in our experiments, were made from non-ionic surfactants Span 60 (sorbitane-monostearate) and Solulan C24 (cholesteryl-poly-24-oyxyethylene-ether), and cholesterol as shown on Fig. 3.

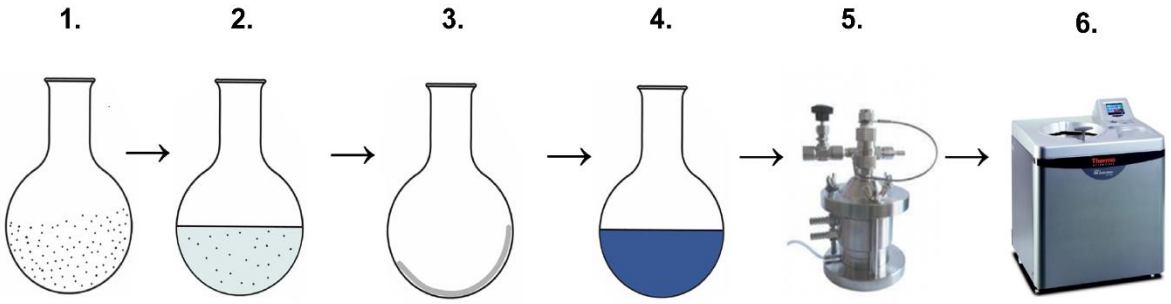


***Figure 3.*** *Preparation steps of niosomes: (1-2) dissolving non-ionic surfactants, cholesterol and transporter ligands in ethanol and chloroform, (3) lipid film formation by evaporation of solvents, (4) hydratation of dried lipid film with the solution containing cargo molecules followed by sonication, (5) high pressure extrusion, (6) ultracentrifugation.*

Niosomes were functionalized with N-dodecyl-β-D-glucopyranose (GP), dodecanoyl-alanine (A) or pegylated-GSH (GSH) to prepare targeted niosomes (N-GP, N-A, N-GSH) or dual-targeted NPs (N-A-GP, N-A-GSH, N-GP-GSH). The red fluorescent EBA was encapsulated in niosomes as a model cargo molecule. The NPs were characterized for particle size and zeta potential using dynamic light scattering. To examine the stability of particles the physico-chemical properties of niosome samples have been followed for 6 month. The amount of the encapsulated EBA in the NPs was determined by a spectrofluorometer. The niosomes were visualized by transmission and atomic force microscopy.

#### 3.5.2. Viability and cellular uptake measurements

The kinetics of RBECs reaction to niosome treatment was monitored in real time by impedance measurement. To measure the cellular uptake of niosomes confluent monlayers of RBECs were incubated with single or dual-targeted niosomes (10 mg/mL concentration, 4 ºC or 37 ºC). To elucidate the uptake mechanisms of targeted niosomes cells were treated with sodium azide, a metabolic inhibitor (1 mg/mL) or with inhibitors of endocytosis, filipin (6 μM, 15 min) or cytochalasin D (20 μM, 1 h). To study the role of the surface charge in the cellular uptake of NPs the surface glycocalyx of RBECs was digested with neuraminidase (1 U/mL, 1h), or the cells were treated with TMA-DPH, a cationic lipid (54 μM, 30 min) before the uptake experiments. At the end of the uptake experiments the cells were washed, lysed and the fluorescent signal in the samples was detected by a spectrofluorometer.

### 3.5.3. Permeability measurements on the BBB co-culture model

To determine the permeabilty of the cargo encapsulated in NPs across the BBB triple co-culture model the cells were treated in the upper, donor compartment with single or dual-targeted niosomes for 4 h. After incubation samples were collected from the lower, acceptor compartments and measured with a spectrofluorometer at 584 nm excitation and 663 nm emission wavelengths, then the $P_{app}$ values of the EBA cargo were calculated.

### 3.5.4. Membrane fluidity measurements on cells treated with niosomes

To measure the plasma membrane fluidity, RBECs grown in culture dishes were treated with N and N-A-GSH samples for 4 h at 37°C in a $CO_2$ incubator. Cells were labeled with TMA-DPH, a fluorescent lipid probe (0.2 μM, 5 min). Fluorescence anisotropy was measured on a T-format fluorescence spectrometer, excitation and emission wavelengths were 360 and 430 nm, respectively. Anisotropy data were acquired in every second for 5 min, then benzyl alcohol (50 mM), a strong membrane fluidizer, was added and data were acquired for another 5 min.

### 3.5.5. *In vivo* experiments

Ten-week old male CD1-Foxn1nu nude mice were used for *in vivo* imaging. The different niosomes (N, N-A, N-GP, N-A-GP), containing EBA as cargo, were injected intravenously. A time domain *in vivo* small animal fluorescence imager Optix™ was used to monitor the brain penetration of the red fluorescent EBA in real-time and over several time points in the same animal. The fluorescent signal was detected over the brain of living anesthetized mice in 0.5 mm steps. For fluorescence detection, a time-correlated single-photon counting system (TCSPC-130) was used.

### 3.5.6. Statistical analysis

Data are presented as means ± SEM or SD. Values were compared using unpaired *t*-test, one-way or two-way analyses of variances (ANOVA) following Dunnett or Bonferroni multiple comparison posttests (GraphPadPrism 5.0). Changes were considered statistically significant at $P < 0.05$. All experiments were repeated at least two times and the number of parallel samples was 4-10.

## 4. RESULTS

### 4.1. Expression of selected solute carrier genes coding nutrient transporters

We verified the expression of genes for SLC transporters carrying glucose, alanine and biotin in freshly isolated rat brain microvessels, RBECs from triple culture BBB model and hCMEC/D3 cells (Fig. 4). Among the carriers of glucose, the expression level of the gene *GLUT1*, coding the predominant glucose transporter at the BBB, was the highest. From the tested neutral amino acid transporters the mRNA level of *SNAT2* was the highest in all models. The expression levels of the *SMVT* gene were similar in the BBB model and the hCMEC/D3 cells. From the tested ten genes only in three cases, for *GLUT5*, *SNAT1* and *SNAT5* were transcript levels lower in the BBB model than in brain microvessels and/or hCMEC/D3 cells (Fig. 4).

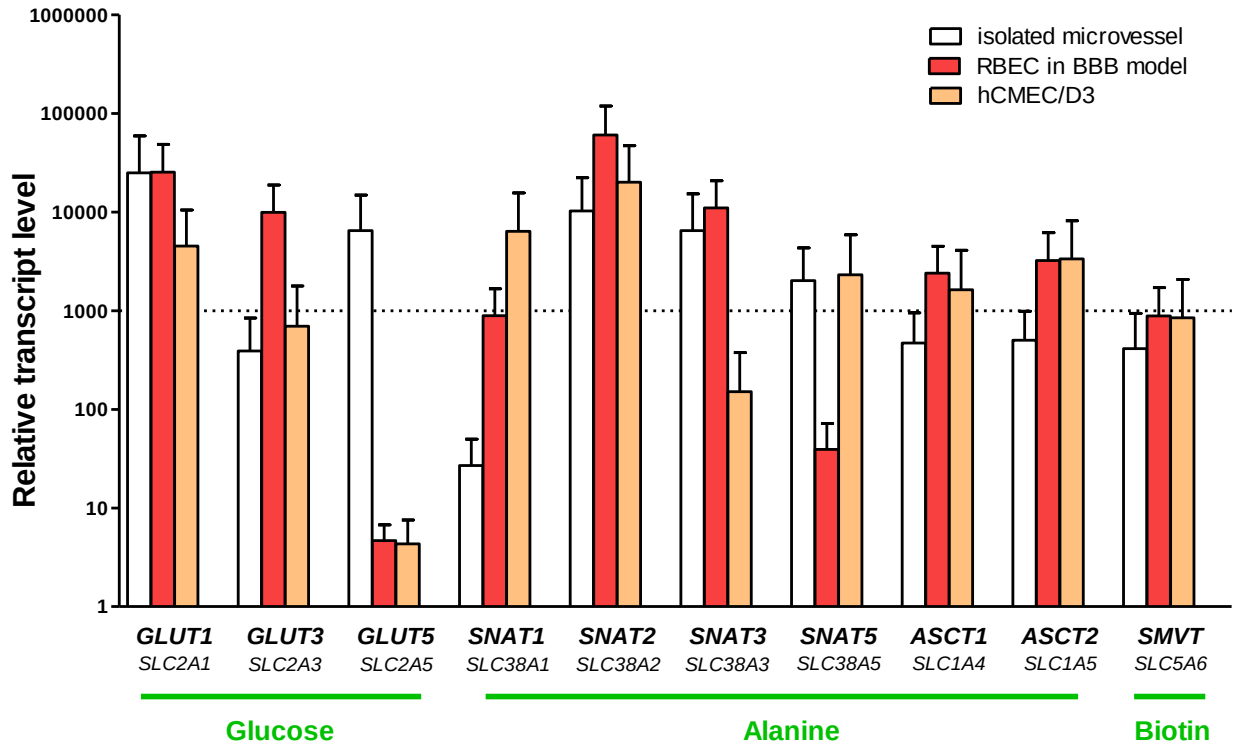


***Figure 4.*** *Expression of genes encoding solute carriers for glucose, alanine and biotin in isolated rat brain microvessels, primary rat brain endothelial cells co-cultured with rat pericytes and astrocytes, and hCMEC/D3 human brain endothelial cell line.*

### 4.2. Results with solid nanoparticles

#### 4.2.1. Characterization of the non-targeted and targeted solid nanoparticles

The fluorescent SNPs were labeled with biotin and glutathione targeting ligands (Fig. 5). The size of SNPs varied between 93-120 nm. All SNP groups had low polydispersity index, indicating a relatively narrow size distribution. The average zeta potential for both targeted particles was very similar (−23 mV). The charge of the non-labeled SNP was less negative. The particles had mostly spherical shapes, but some SNPs were elongated. No aggregation was visible.

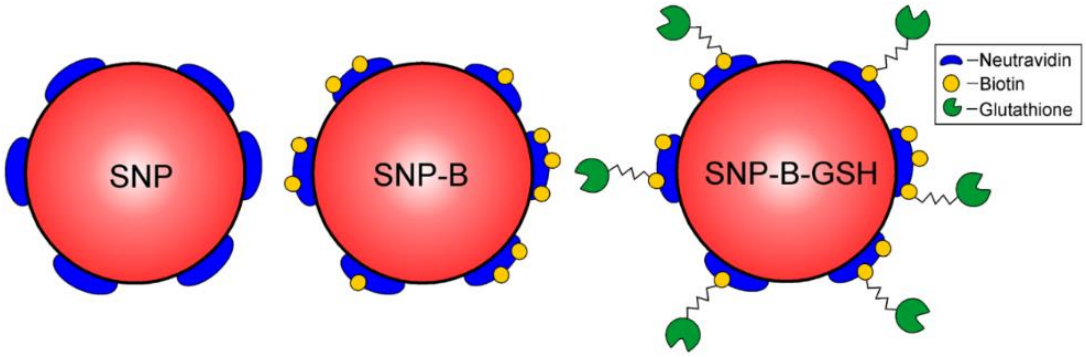


***Figure 5****. Schematic drawing of non-targeted (SNP), biotin- (SNP-B) and glutathione-labeled (SNP-B-GSH) solid nanoparticles.*

#### 4.2.2. Viability measurement and cellular uptake of solid nanoparticles

Incubation of the human brain endothelial cell monolayers with SNP and SNP-B in the 10-1000 μg/mL concentration range for 24 h had no effect on cell viability assessed by MTT dye conversion test. For further experiments we selected the 150 μg/mL concentration for all three SNPs, which can be considered as non-toxic.

The uptake of SNPs in hCMEC/D3 was tested at two time points (4 and 8 h). After 8 h incubation the uptake of all tested nanoparticles was significantly higher compared to the 4 h group. Importantly, the uptake of the biotin- and glutathione-targeted SNPs was significantly increased; it was two times higher than the uptake of the non-targeted particle (Fig. 6).

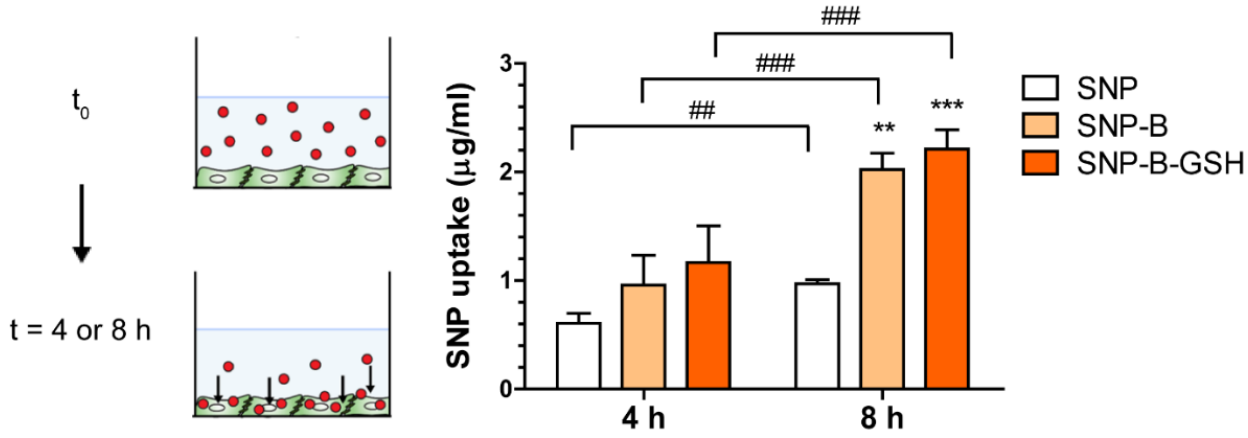


***Figure 6.*** *The uptake of non-targeted (SNP), biotin-labeled (SNP-B) and glutathione-labeled (SNP-B-GSH) solid nanoparticles in brain endothelial cells after 4 or 8 h incubation. The concentration of SNPs was 150 µg/mL in all groups. Values presented are means ± SEM. Statistical analysis: two-way ANOVA followed by Bonferroni posttest, where **P < 0.01; ***P < 0.001, compared to SNP treated group, ##P < 0.01; ###P < 0.001, compared to the 4 h incubation group; n = 4–6.*

### 4.2.3. Penetration of solid nanoparticles across brain endothelial monolayers

All SNPs crossed the brain endothelial layers in the permeability tests but at different extent (Fig. 7). After 8 h incubation the $P_{app}$ of biotin targeted SNPs was 2.8 fold higher than that of the non-targeted SNPs. The penetration of the GSH targeted nanoparticles was the highest: a significant, 5.8 fold increase was measured as compared to the unlabeled SNP group.

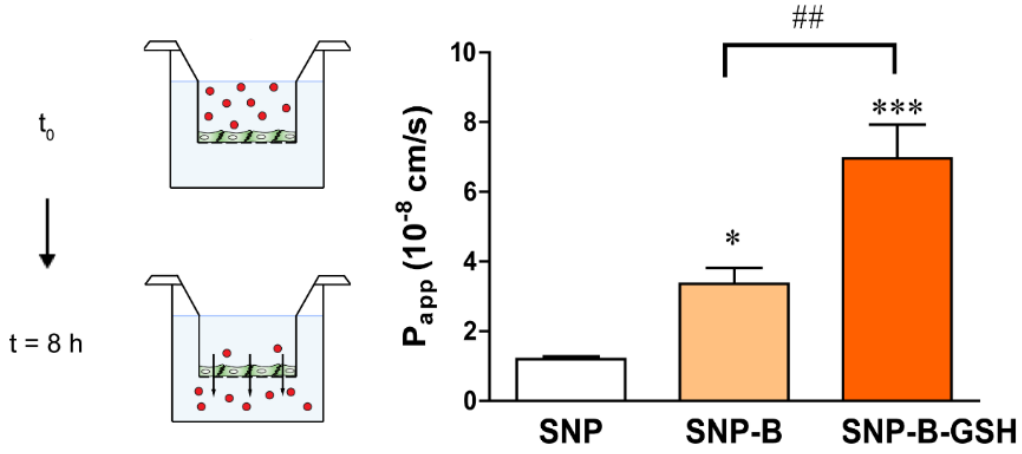


***Figure 7****. Permeability assay for targeted and non-targeted SNPs (150 µg/mL, 8 h) across hCMEC/D3 cell monolayers. Values presented are means ± SEM. Statistical analysis: one-way ANOVA followed by Bonferroni posttest. *P < 0.05, ***P < 0.001, compared to non-labeled SNP treated group; ##P < 0.01, compared to biotin-labeled SNP treated group, n = 6.*

### 4.2. Results with niosomes

#### 4.2.1. Characterization of non-targeted and targeted niosomes

Seven types of niosomes (non-targeted, N), single ligand targeted (N-GP, N-A, N-GSH), and dual-ligand targeted (N-A-GSH, N-A-GP, N-GP-GSH) were prepared with the fluorescent EBA cargo (Fig. 8).

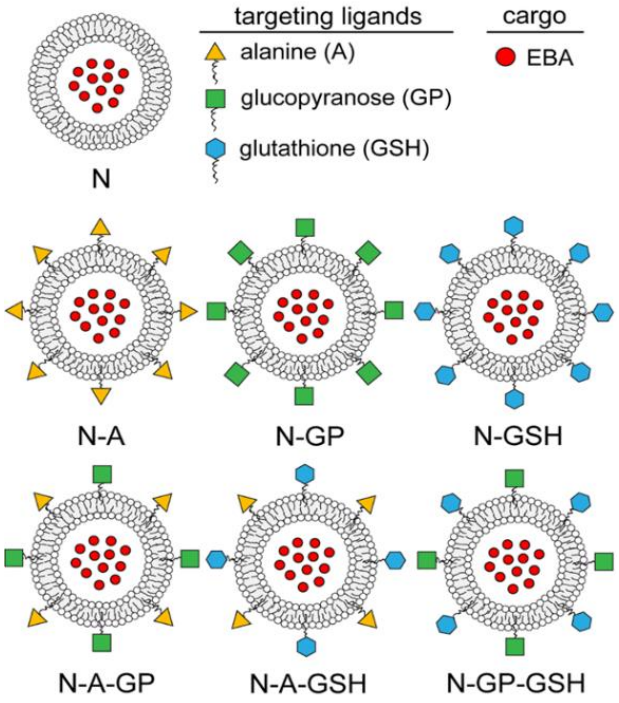


***Figure 8****. Schematic drawing of non-targeted (N), single ligand targeted (N-A: alanine, N-GP: glucopyranose, N-GSH: glutathione) and dual-targeted niosomes (N-A-GP: glucose-alanine, N-A-GSH: alanine-glutathione, N-GP-GSH: glucose-glutathione). EBA: Evans blue-albumin complex.*

The average diameter of niosomes varied between 92 and 107 nm. All groups had low polydispersity index, indicating a narrow size distribution. The zeta potentials of niosomes were between −3 and −4 mV, except those decorated with GSH ligand (N-GSH, N-A-GSH, N-GP-GSH), which had a more negative surface charge, around −7mV. The encapsulation efficiency of the cargo EBA was in the range of 4.6–10.4%. The amount of the encapsulated large hydrophilic biomolecule EBA was between 0.5 and 1.1 mg/100 mg nanoparticle total weight.

The morphology of the NPs was spherical as observed by transmission electron microscopy (Fig. 9A) and atomic force microscopy (Fig. 9B). No aggregation was visible.

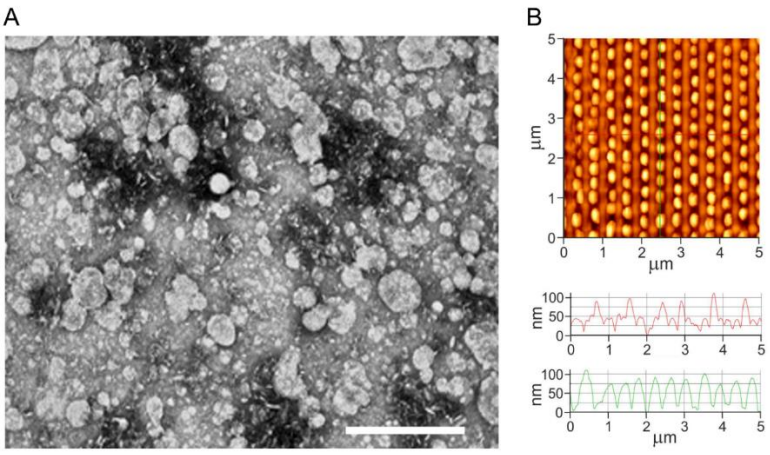


***Figure 9.*** *(A) Transmission electron microscopy image of niosomes, bar: 500 nm. (B) Atomic force microscopy image of niosomes.*

The stability of non-targeted niosomes loaded with EBA was followed for six months. The size of niosomes changed from 92.8 ± 1.8 nm to 119.5 ± 1.9 nm during this period. At 6 months the physico-chemical properties have changed minimally. Based on these data the niosome preparations can be considered as stable regarding size, encapsulated cargo and aggregation for at least 6 months.

### 4.2.2. Viability and cellular uptake measurements

Incubation of RBECs with non-targeted or targeted niosomes in the 0.3–10 mg/mL concentration range for 4h did not decrease the impedance of cell layers reflecting good cell viability. For further experiments we selected the 10 mg/mL concentration, which can be considered as a safe concentration for all niosome groups. The uptake of the large hydrophilic free EBA was very low in brain endothelial cells, only 1.5% of the EBA uptake measured in cells treated with non-targeted niosome (N) containing the cargo (Fig.10).

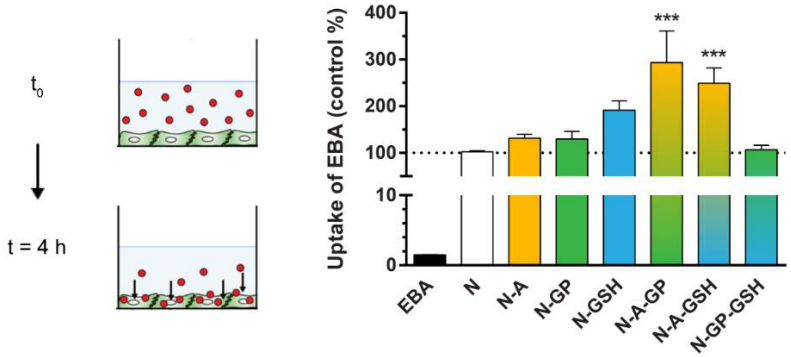


***Figure 10.*** *The uptake of EBA in brain endothelial cells treated with non-targeted (N), single- (N-A, N-GP, N-GSH) and dual-targeted (N-A-GP, N-A-GSH, N-GP-GSH) niosomes (4 h). Values presented are means ± SEM. Statistical analysis: ANOVA followed by Dunnett's posttest, where ***P < 0.001, compared to non-targeted N group; n=10.*

As compared to non-targeted niosomes, the uptake of EBA in RBECs treated with nanovesicles decorated with alanine, glucopyranose or glutathione was higher. The presence of dual-ligands increased the cellular concentration of EBA in brain endothelial cells in the case of N-A-GP and N-A-GSH groups, but not in the N-GP-GSH group (Fig. 10).

### 4.2.3. Penetration of the cargo of targeted niosomes across BBB co-culture model

The permeability of the BBB model for EBA was also very low reflecting a tight barrier (Fig. 11). The encapsulation of EBA in non-targeted niosomes (N) increased the permeability of the cargo through RBECs. Labeling the particles with single ligands resulted in further increase in the penetration of EBA across the BBB model. The amount of EBA cargo that crossed brain endothelial cells was increased 17-fold in case of the N-A-GSH group and 14-fold in the N-A-GP group as compared to the EBA group (Fig. 11). The combination of GP-GSH ligands was not efficient to elevate EBA penetration across the BBB model. Based on the results, the N-A, N-GSH and N-A-GSH groups were selected for further *in vitro* experiments.

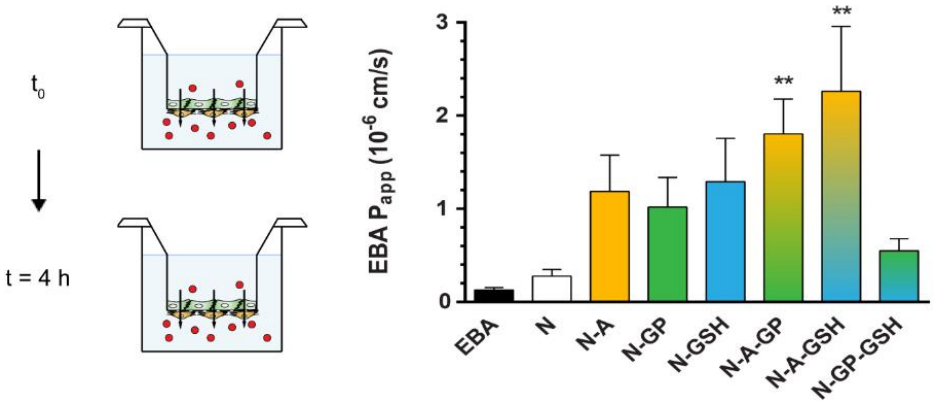


***Figure 11.*** *Permeability of albumin cargo across the BBB culture model after treatment with different niosomes (10 mg/mL, 4h). Values presented are means ± SEM. Statistical analysis: ANOVA, Dunnett's posttest. **P < 0.01, compared to non-targeted N group; n=10.*

### 4.2.6. Cellular uptake: temperature dependence and metabolic inhibition

At 37 °C the EBA uptake was significantly higher in all targeted nanovesicle groups compared to the non-targeted group (Fig. 12). Decreased EBA uptake was seen in RBECs at 4 °C and after treatment of the cells with metabolic inhibitor sodium azide in all targeted groups.

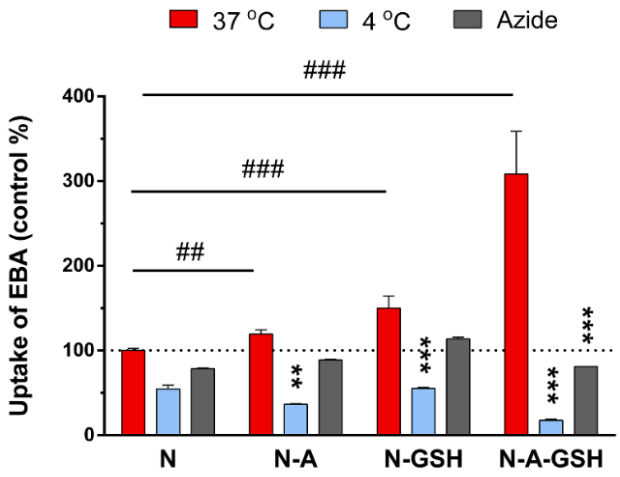


***Figure 12.*** *The effect of temperature and metabolic inhibitor sodium azide (0.1%) on the uptake of EBA cargo in brain endothelial cells after 4h incubation with non-targeted (N), alanine-targeted (N-A), glutathione-targeted (N-GSH) and alanine-glutathione-targeted (N-A-GSH) niosomes. Values presented are means ± SEM. Statistical analysis: two-way ANOVA, Bonferroni posttest. *P < 0.5; **P < 0.01; ***P < 0.001, compared to first column of each groups, ###P < 0.001, compared to N treated group; n=4–6.*

### 4.2.7. Cellular uptake: inhibition of endocytosis

Two inhibitors of endocytosis were used to further elucidate the mechanism of cellular uptake of EBA in cells treated with dual-targeted N-A-GSH particles (Fig. 13). Filipin, which inhibits lipid raft/caveolae-mediated endocytosis (Fig. 13B), slightly, but statistically significantly decreased the uptake of cargo in RBECs (Fig. 13A). Cytochalasin-D, a commonly used inhibitor of endocytosis which blocks F-actin depolymerization (Fig. 13B), also induced a partial, but significant inhibition of EBA uptake (Fig. 13A).

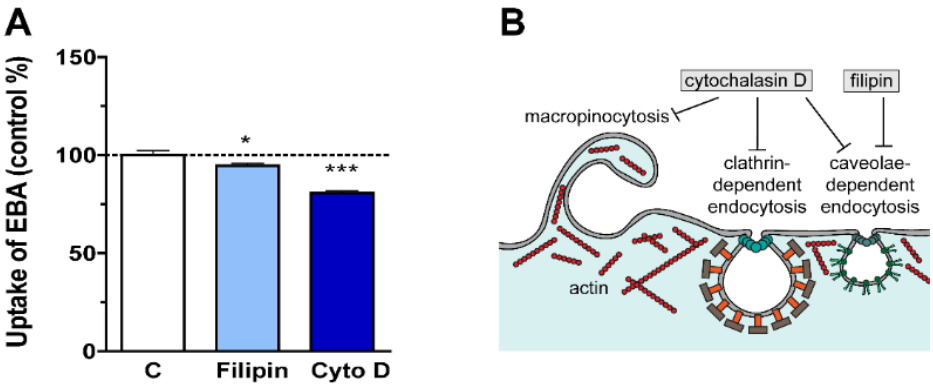


***Figure 13****. (A) Inhibition of the uptake of EBA cargo with filipin (6 μM) or cytochalasin D (20 μM) in rat brain endothelial cells after 4 h incubation with alanine-glutathione dual-targeted niosomes (N-A-GSH). Values presented are means ± SEM. Statistical analysis: ANOVA followed by Dunnett's posttest. *P < 0.5; ***P < 0.001, compared to the control group; n=6. (B) Schematic drawing of the effect of cytochalasin D and filipin.*

### 4.2.8. Cellular uptake: modification of cell surface charge

We modified the surface charge of cultured brain endothelial cells by digestion of the surface glycocalyx with neuraminidase enzyme and treatment with a cationic lipid, TMA-DPH. Surface charge alterations in RBECs did not affect the cellular uptake of EBA after treatment with non-targeted NPs as compared to the control, untreated group (Fig. 14A).

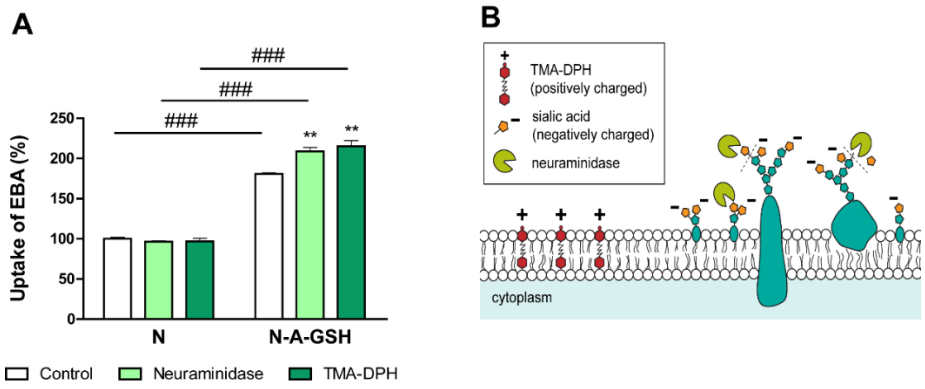


***Figure 14.*** *(A) The effect of neuraminidase (1 U/mL) and TMA-DPH (54 μM) on the uptake of EBA cargo in brain endothelial cells incubated with non-targeted (N) and alanine-glutathione dual-targeted niosomes (N-A-GSH). Statistical analysis: two-way ANOVA, Bonferroni posttest. **P < 0.01 compared to first column of each groups; ###P < 0.001, compared to N treated groups; n=6. (B) Schematic drawing on the effect of TMA-DPH and neuraminidase on the surface charge of RBEC.*

In contrast, both modifications increased the uptake of EBA in brain endothelial cells after incubation with N-A-GSH niosomes (Fig. 14). The uptake of EBA was increased by 16%, after treatment of RBECs with neuraminidase and by 19% after incubation with TMA-DPH, as compared to untreated cells in the N-A-GSH nanoparticle group.

### 4.2.9. Interaction of nanovesicles with brain endothelial cells: plasma membrane fluidity

The fluorescence anisotropy measured in a single cell suspension of living brain endothelial cells was significantly decreased after 4h treatment with N and N-A-GSH nanovesicles (Fig. 15A) indicating increased cell membrane fluidity and a fusion process (Fig. 15B). The membrane fluidizer benzyl alcohol (30 mM) quickly and greatly reduced the TMA-DPH fluorescence anisotropy after 3 min compared to the control and niosome treated groups indicating maximal plasma membrane fluidity.

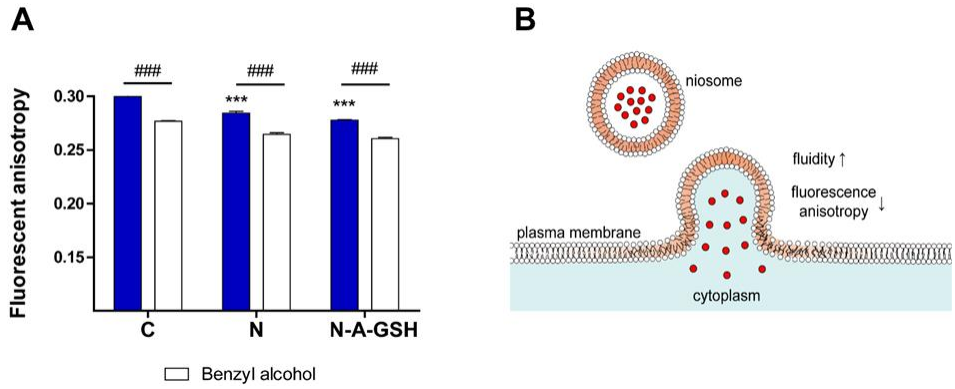


***Figure 15***. *(A) The effect of non-targeted (N) and alanine-glutathione dual-targeted niosomes (N-A-GSH), and benzyl alcohol (30 mM) on plasma membrane fluidity measured by fluorescence anisotropy of living brain endothelial cells in suspension. Values presented are means ± SEM. Statistical analysis: two-way ANOVA, Bonferroni posttest. ***P < 0.001, all groups were compared to non-treated control (C); ###P < 0.001, compared to first column of each groups, n=3. (B) Schematic drawing on the fusion of a niosome with cellular plasma membrane.*

### 4.2.10. Imaging of EBA cargo in mice after intravenous injection of targeted niosomes

The brain penetration of the red fluorescent EBA was measured by *in vivo* imaging in nude mice. In animals which were injected with free EBA there was no significant elevation in the signal intentsity in the brain area during the experiment (Fig. 16). Encapsulation of EBA in non-targeted niosomes resulted in enhanced brain fluorescence intensity. The fluorescent signal in the brain area was further increased in the single ligand targeted N-A and N-GP groups, while in the dual-ligand targeted N-A-GP group it was the highest, as compared to all groups at all time points (Fig. 16). The differences between targeted, dual-ligand targeted and non-targeted niosomes were still visible at 24 h.

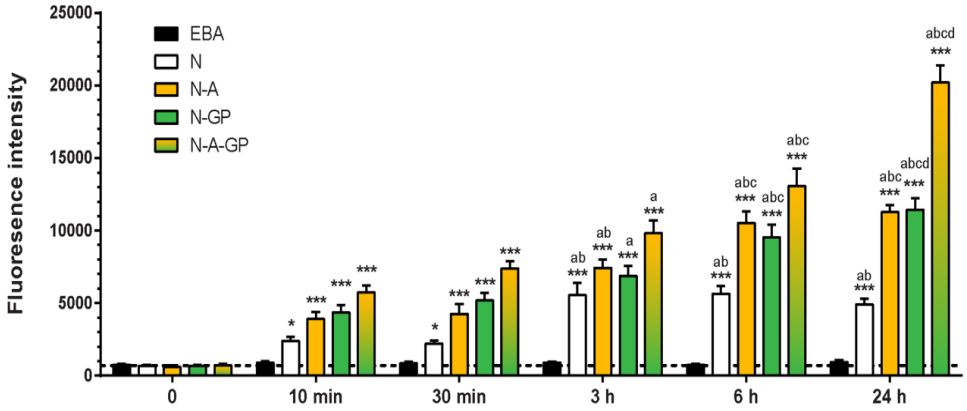


***Figure 16.*** *Fluorescence intensity of EBA in the brain regions of mice after injection of free EBA or EBA encapsulated in non-targeted (N), single- (N-A, N-GP) or dual-targeted (N-A-GP) niosomes measured by optical imaging. Values presented are means ± SD. Statistical analysis: two-way ANOVA, Bonferroni posttest.* P < 0.5; **P < 0.01; ***P < 0.001, as compared to the EBA-treated group within each time point; a: as compared to the 10 min, b: as compared to the 30 min, c: as compared to the 3h, d: as compared to the 6 h time points within each group, n=3–4.*

## 5. SUMMARY

NPs for drug targeting across the BBB are promising candidates to increase the brain penetration of biopharmacons for treating CNS diseases. Effective targeting of NPs can only be achieved by exploiting the BBB specific physiological transport pathways. Despite the abundance of carrier mediated transporters at the BBB this pathway is still underresearched for drug delivery.

Solute carriers functioning as nutrient transporters are expressed at high levels in brain endothelial cells and show a specific pattern at the BBB. Our hypothesis was, that targeting SLCs expressed at the BBB can enhance nanoparticle uptake and permeability across brain endothelial cells, and using ligands for two different SLCs at the same time could further increase nanoparticle penetration. The aim of our studies was to identify and test SLC transporter ligands and glutathione as single or dual BBB targeting molecules for solid and vesicular NPs.

In our first study we tested biotin-labeled solid NPs and compared them to glutathione-labeled NPs on an *in vitro* BBB model. Fluorescent polystyrene NPs were derivatized and investigated on human brain endothelial cells. We verified that hCMEC/D3 cells express mRNA for sodium-dependent multivitamin transporter (SMVT/SLC5A6) responsible for the BBB transport of biotin. Biotin as a ligand increased the uptake and the transfer of NPs across brain endothelial cells. Glutathione could further increase NP permeability across the BBB model, supporting its use as a brain targeting vector.

In the second series of experiments vesicular NPs were investigated. High mRNA expression levels for hexose and neutral amino acid transporting SLCs were found in isolated rat brain microvessels and a rat primary cell based co-culture BBB model. Niosomes, nanovesicles prepared from non-ionic surfactants, were decorated with glutathione and SLC ligands glucopyranose and alanine, and loaded with Evans blue-albumin complex as a large biomolecule model cargo. The presence of targeting ligands on niosomes, especially dual labeling, increased the uptake of the cargo molecule in cultured brain endothelial cells. This cellular uptake was temperature dependent and decreased following application of a metabolic inhibitor, sodium azide, and endocytosis blockers filipin and cytochalasin D. Turning the negative surface charge of brain endothelial cells more positive with a cationic lipid or digesting the glycocalyx with neuraminidase elevated the uptake of the cargo encapsulated in targeted nanocarriers. Niosomes increased plasma membrane fluidity, suggesting the fusion of nanovesicles with the endothelial cell membranes. Targeting ligands elevated the permeability

of the cargo across the BBB in the culture model and in mice, and dual-ligand decoration of niosomes was more effective than single ligand labeling. As a conclusion, our data indicate that ligands of multiple SLC transporters can be exploited for BBB targeting of NPs.

## 6. PUBLICATIONS RELATED TO THE SUBJECT OF THE THESIS

**I.** Veszelka S, **Mészáros M**, Kiss L, Kóta Z, Páli T, Hoyk Z, Bozsó Z, Fülöp L, Tóth A, Rákhely G, Deli MA.
Biotin and glutathione targeting of solid nanoparticles to cross human brain endothelial cells.
*Current Pharmaceutical Design.* 2017 Jul 27; 23:4198-4205.
IF: 2.86, Q1

**II.** Veszelka S, Tóth A, Walter FR, Tóth AE, Gróf I, **Mészáros M,** Bocsik A, Hellinger É, Vastag M, Rákhely G, Deli MA.
Comparison of a rat primary cell-based blood-brain barrier model with epithelial and brain endothelial cell lines: gene expression and drug transport.
*Frontiers in Molecular Neuroscience*. 2018 May 22; 11:166.
IF: 3.902, Q1

**III.** **Mészáros M,** Porkoláb G, Kiss L, Pilbat AM, Kóta Z, Kupihár Z, Kéri A, Galbács G, Siklós L, Tóth A, Fülöp L, Csete M, Sipos Á, Hülper P, Sipos P, Páli T, Rákhely G, Szabó-Révész P, Deli MA, Veszelka S.
Niosomes decorated with dual ligands targeting brain endothelial transporters increase cargo penetration across the blood-brain barrier.
*European Journal of Pharmaceutical Sciences*. 2018 Oct 15; 123:228-240.
IF: 3.466, Q1

## OTHER PUBLICATION

**I.** Sántha P, Veszelka S, Hoyk Z, **Mészáros M**, Walter FR, Tóth AE, Kiss L, Kincses A, Oláh Z, Seprényi G, Rákhely G, Dér A, Pákáski M, Kálmán J, Kittel Á, Deli MA.
Restraint stress-induced morphological changes at the blood-brain barrier in adult rats.
*Frontiers in Molecular Neuroscience.* 2016 Jan 14; 8:88.
IF: 5.08, Q1

## 8. ACKNOWLEDGEMENTS

I am grateful to my supervisors Prof. Mária Deli and Dr. Szilvia Veszelka for their scientific guidance, encouragement and support throughout my Ph.D. studies.

I thank Prof. Pál Ormos and Prof. Ferenc Nagy, the director generals of the Biological Research Centre, Prof. László Zimányi, director of the Institute of Biophysics, and Dr. László Siklós, head of the Molecular Neurobiology Research Unit for their support.

I am indebted to our cooperating partners Dr. Zoltán Kupihár and Dr. Zsolt Bozsó for the synthesis of targeting ligands, Dr. Ana-Maria Pilbat for the membrane fluidization experiments; Dr. Zoltán Kóta for the fluorometric measurements; Dr Lóránd Kelemen for the scanning electronmicroscopy study; Dr. Lívia Fülöp and Dr. László Siklós for the transmission electronmicroscopy studies; Dr. Mária Csete and Dr. Áron Sipos for the atomic force microscopy study; Dr. Gábor Galbács and Albert Kéri for the determination of lanthanum content of niosomes and Dr. Petra Hülper for her help in the *in vivo* imaging experiments.

I am grateful to my previous and present laboratory colleagues, Dr. Petra Sántha, Dr. Lóránd Kiss, Dr. Zsófia Hoyk, Dr. Fruzsina Walter, Dr. Alexandra Bocsik, Dr. András Harazin, Ilona Gróf, Ana Raquel Pato Santa Maria, Lilla Barna, Beáta Barabási, Judit Vigh, Adrián Klepe, Anikó Szecskó for excellent teamwork and sharing the excitement of research and discovery.

I am very thankful to Gergő Porkoláb for his kind help in my experimental work.

I also thank the members of the Institute of Biophysics for their help and friendship.

Finally, I am especially thankful to my parents, my grandparents, my brother and my friends for their love and untiring support during my studies.

*The research was supported by the Hungarian Scientific Research Fund (OTKA/NKFIH 105622), by the National Research, Development and Innovation Office (GINOP-2.2.1-15-2016-00007, GINOP-2.3.2-15-2016-00060 and EFOP-3.6.1-162016-00008).*